JOURNAL OF THERMOPHYSICS AND HEAT TRANSFER
Vol. 24, No. 1, January–March 2010

Effect of Return Inlet on Thermal Stratification in a Rocket Tank

Xianghua Cheng,* Yanzhong Li,† Erfeng Chen,‡ and Cui Li§
Xi'an Jiaotong University, Xi'an 710049, People's Republic of China

DOI: 10.2514/1.42201

Thermal stratification in a rocket liquid-oxygen tank with a natural circulation precooling loop is numerically analyzed under different return inlet locations and influx angles. It is found that the heat convection is dominant in the bulk above the return inlet location and that the heat conduction becomes primary below the location. The axial thermal stratification exists in the whole range of the tank, and the radial stratification appears mainly in the bottom. The stratifications are influenced by the selection of the return inlet location and influx angle, and the optimal values of the return inlet location at $hi/L = 0.3$ and the influx angle of 30 deg are determined.

Nomenclature

C_0	=	blackbody radiation coefficient, $W \cdot m^{-2} \cdot K^{-4}$
c_p	=	specific heat, $kJ \cdot kg^{-1} \cdot K^{-1}$
d	=	outer diameter of tank, m
F	=	area, m^2
g	=	acceleration due to gravity, $m \cdot s^{-2}$
H	=	tank height, m
h	=	enthalpy, $kJ \cdot kg^{-1}$
h_A, h_B	=	convection heat transfer coefficient of exterior, $W \cdot m^{-2} \cdot K^{-1}$
hi	=	return inlet height, m
$h(z)$	=	height, m
k	=	turbulent kinetic energy, $m^2 \cdot s^{-2}$
L	=	liquid oxygen height, m
$\dot{m}$	=	rate of mass transfer, $kg \cdot s^{-1}$
Nu	=	Nusselt number
Pr	=	Prandtl number
p	=	pressure, Pa
q	=	heat flux, $W \cdot m^{-2}$
R	=	tank radius, m
R_c	=	coupled thermal resistance of convection radiation, $m^2 \cdot K \cdot W^{-1}$
Re	=	Reynolds number
R_{iso}	=	thermal resistance of insulation layer, $m^2 \cdot K \cdot W^{-1}$
R_{met}	=	thermal resistance of tank wall, $m^2 \cdot K \cdot W^{-1}$
T	=	absolute temperature, K
T_{in}	=	the inner wall temperature of tank, K
T_m	=	characteristic temperature of atmosphere, K
T_{max}	=	saturation temperature corresponding to the bottom outlet pressure, K
T_{mid}	=	the exterior surface temperature of insulation material, K
T_{min}	=	saturation temperature corresponding to initial ullage pressure, K
T_{out}	=	temperature of atmosphere, K
T_{sat}	=	saturation temperature, K
t	=	time, s
u	=	x component of velocity, $m \cdot s^{-1}$, Eqs. (9–15); uniform velocity, $m \cdot s^{-1}$, Eqs. (A1–A3)
u_f	=	wind velocity, $m \cdot s^{-1}$
v	=	y component of velocity, $m \cdot s^{-1}$
v_f	=	kinematic viscosity, $m^2 \cdot s^{-1}$
x, y	=	coordinate variables
α	=	return influx angle; void fraction, Eq. (18)
β	=	thermal expansion coefficient, K^{-1}
ε	=	rate of dissipation of turbulent kinetic energy, $m^2 \cdot s^{-3}$
θ	=	dimensionless excess temperature, $(T - T_{min})/(T_{max} - T_{min})$; the slope angle of pipeline, Eq. (A2)
λ	=	heat conduction coefficient, $W \cdot m^{-1} \cdot K^{-1}$
μ	=	dynamic viscosity, $Pa \cdot s$
ρ	=	density, $kg \cdot m^{-3}$
Φ	=	heat transfer rate, W
φ, δ	=	any dependent variable

Received 14 November 2008; revision received 5 June 2009; accepted for publication 31 August 2009.

*State Key Laboratory of Multiphase Flow in Power Engineering, School of Energy and Power Engineering; xjtucxh@yahoo.com.cn.

†State Key Laboratory of Multiphase Flow in Power Engineering, School of Energy and Power Engineering; yzli-epe@mail.xjtu.edu.cn (Corresponding Author).

‡State Key Laboratory of Multiphase Flow in Power Engineering, School of Energy and Power Engineering.

§State Key Laboratory of Multiphase Flow in Power Engineering, School of Energy and Power Engineering.

I. Introduction

CRYOGENIC liquid oxygen is adopted as the propellant of the new-style launch vehicle, and the propellant tank with natural circulation precooling loop is considered as the fuel storage and supply equipment during the ground parking and flight. Because of the natural convection and aerodynamic heating, there is a large temperature difference between fluid inside the tank and the surroundings. The liquid oxygen can be heated and flows along the sidewall of the tank toward the upper regions to the liquid–gas interface. This process generally results in the thermal stratification along the height of the tank [1–3]. The thermal stratification phenomenon in the cryogenic propellant tank of a launch vehicle is an important design consideration because of its direct influence on pump cavitation, vaporization, tank pressure rise and the selection of venting devices, insulations and tank structure, etc. Thermal stratification is affected by many factors, such as the initial liquid aspect ratio, variable liquid properties, operating pressure, thermal performance, and tank structure. In a new-style launch vehicle, the propellant pump and engine are precooled using subcooled liquid oxygen through a natural circulation loop before launch. Consequently, the effects of the return inlet location and influx angle on thermal stratification should be taken in account in the design of the precooling system.

Several experimental and numerical studies on thermal stratification in a cryogenic vessel have been reported in the literature. Khurana et al. [4] investigated the thermal stratification in ribbed liquid hydrogen storage tanks and a significant decrease in the degree of thermal stratification was demonstrated by improvising transverse

wall ribs on the inner cylindrical surfaces of large liquid hydrogen storage tanks. Navickas and Douglas [5] predicted the thermal stratification in a liquid tank by a finite difference computing method and it was shown that baffles are very effective in destratifying the fluid temperature. Zhang and Li [6] described the vorticity-stream function method as the numerical simulation for the thermal stratification of LH_2; the results of interface temperature were correlated with the heat flux, liquid level, and time. A scaled-down model study of convective heat transfer in a rectangular glass tank was investigated using water as the medium fluid by Das et al. [7], and a numerical study was completed in a cylindrical column filled with liquid hydrogen and heated from the sides. Tatom et al. [8] found that bottom and side heating of the tank produced noticeably different stratification patterns using schlieren photographs. Manalo [9] studied the onset and growth of the natural circulation and thermal stratification inside a cryogenic propellant storage tank due to heat transfer from surroundings and the effect of variable fluid properties, initial subcooling, operating pressure, and initial liquid aspect ratio on thermal stratification were numerically investigated. In addition, there have been several studies on thermal stratification in solar domestic hot-water systems [10–14] in which the effects of water inlet location and velocity on thermal stratification and temperature distribution in the tank were studied.

The previous studies basically focused on the thermal stratification in the closed cryogenic tank without drainage and influx fluid. However, in practice, the liquid oxygen tank of a new-style launch vehicle is always connected with a natural circulation loop; the distributions of temperature and velocity field in the tank are more complex than that in a simplified closed tank, especially when considering the effects of return inlet location and influx angle on thermal stratification. Because it is extremely difficult to perform flow visualization in an actual liquid-oxygen tank, in the present work the physical field of the liquid-oxygen tank with natural circulation precooling loop is numerically studied using computational fluid dynamics (CFD) techniques. The distributions of the temperature and velocity fields are depicted and the development of thermal stratification is investigated. The heat transfer mechanisms in different regions and the effects of return inlet location and influx angle on thermal stratification are analyzed. The conclusions offer the academic foundation for the propellant system design of new-style launch vehicles.

II. Tank with Natural Circulation Precooling Loop

A. Principle of Natural Circulation Precooling

The cryogenic liquid oxygen is adopted as the propellant for the new-style launch vehicle, and so the rocket engine and pipelines must be precooled before launch due to the peculiar performance of cryogenic liquid oxygen. The cryogenic propellant tank with the natural circulation precooling loop is sketched in Fig. 1. The precooling loop includes the feeding fall pipeline from the tank bottom down to the engine and pump body and the return pipeline from the pump body back up to the liquid-oxygen tank, and other accessorial devices attached to the loop.

There is a large temperature difference between the cryogenic liquid and pipeline because the engine and pipelines are initially at ambient temperature; hence, the cryogenic liquid is vaporized immediately after entering the loop and the possible flow patterns including the liquid, gas, and gas–liquid two phase flows occur in the loop along the flow direction. With the cooling effect of cryogenic liquid, the wall temperatures of the rocket engine body and pipe decrease and the temperature gradient appears between the pipe wall and external environment, which results in a heat transfer into the pipes and engine body. During the pipe wall temperature decreasing and the occurrence of two-phase flow, the density difference of the two-phase fluid in the feeding fall pipeline and return flow pipeline is regarded as the driving force of natural circulation and maintains the continuous precooling operation. This is also said to be "thermosyphon effect." Finally the gas–liquid two-phase fluid returns to the tank with a higher temperature and velocity.

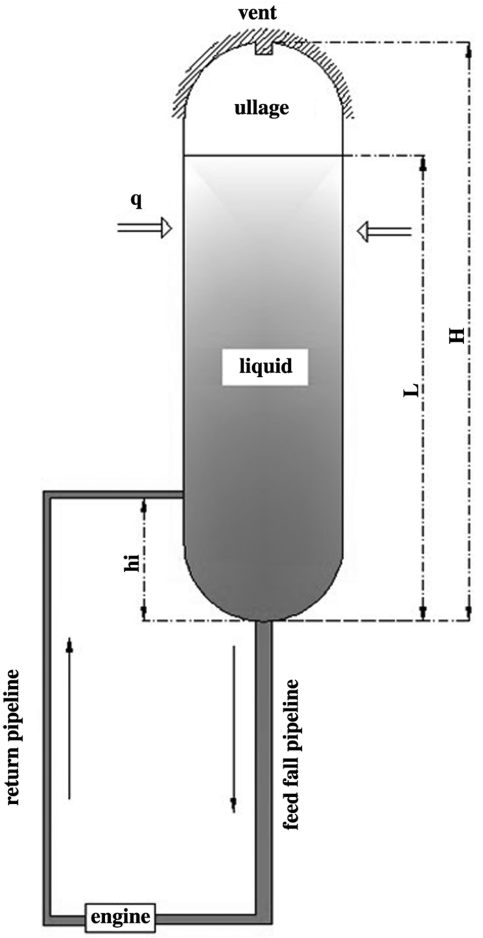

Fig. 1 Propellant tank with natural circulation precooling loop.

B. Tank and Boundary Conditions

The tank is composed of a vertical circular cylinder with two spherical caps in both ends; the correlative parameters for the studied tank are given in Table 1. The four different return inlet locations are selected at $hi/L = 0.1$, 0.2, 0.3, and 0.4, respectively, for the investigation of the location. The aspect ratio of the tank is approximately 5, and the tank diameter is about 10 and 70 times that of the feed fall and return pipes, respectively. For the purpose of heat leakage reduction, the sidewall and bottom of the tank are enwrapped with insulation material of 0.02 m thickness and the top cap is assumed to be perfectly insulated.

The ullage pressure is supposed to be at a constant of 0.12 MPa, the temperature of the initial liquid oxygen in the tank is 91.837 K, and the ambient temperature is 288.15 K. In general, there are three propellant tank boundary conditions: inlet, outlet, and wall. The top vent releases the gas to the environment, which acts to maintain uniform pressure in the ullage space, is regarded as a pressure outlet. The bottom outlet supplies the liquid oxygen for the precooling of the rocket engine during the ground prelaunch. Because the loop precooling operation is an unsteady process, the mass flux of the bottom outlet is calculated iteratively using the one-dimensional

Table 1 Data for the modeling tank

Circular cylinder height, m	11.887
Tank diameter, m	2.25
Liquid height, m	8.02
Spherical cap height, m	0.8
Feeding fall pipe diameter, m	0.22
Return flow pipe diameter, m	0.032
Tank wall thickness, m	0.005
Insulation material	Foaming

homogeneous unbalanced fluid dynamic model [15]; a detailed discussion of the iterative calculation is presented in the Appendix. During the numerical calculation, the two-dimensional value of mass flux transformed from the real calculation is introduced as the condition of the bottom outlet.

The cryogenic fluid returns to the liquid-oxygen tank through the return flow pipeline, and so the return inlet of precooling loop is also treated as an inlet boundary relative to the tank. The whole mass flux of liquid oxygen through the return flow pipeline and the feeding fall pipeline are equal to the negligible loss of liquid oxygen in loop. To investigate the effect of return fluid on the tank field specifically, the inlet conditions of the return fluid are supplied, including the two-phase flow velocity and the void fraction of feeding fluid, which are determined by the calculation of the precooling loop based on one-dimensional unsteady homogeneous models.

The propellant tank is plotted for four calculation regions, including the wall, the ullage space, the bulk, and the liquid–gas interface, for which the heat transfer through the wall is very complicated because of the coupling of different heat transfer mechanisms. The convection and radiation heat transfer of the outside surface, the heat conduction of the insulation material and wall, and the inner convection heat transfer must also be considered. Compared with the external forced convection, the effect of liquid–solid convection heat transfer between the inner wall and liquid oxygen is tremendous. The convection heat transfer coefficient inside is regarded as infinity and the temperatures of the liquid oxygen and inner wall are assumed to be equal. The exterior surface temperature of the tank is unknown and the tentative method is applied to obtain the heat transfer coefficient. The sketch of overall thermal resistance is given in Fig. 2.

The thermal resistances are obtained using a heat conduction formula of the cylinder wall and the value of T_{mid} is required to account iteratively [16]. By assuming a certain value of T_{mid}, the conduction heat transfer rate through the sidewall, Φ, is computed from the relation

$$\Phi = \frac{T_{\text{out}} - T_{\text{in}}}{R_{\text{iso}} + R_{\text{met}} + R_c} \tag{1}$$

According to equivalency principle of thermal transfer quality passing every layer, the convection heat transfer coefficient outside, h_A, is obtained as follows:

$$h_A = \frac{\Phi}{F(T_{\text{out}} - T_{\text{mid}})} \tag{2}$$

where F is exterior surface area of tank.

The characteristic temperature of the atmosphere, T_m, is

$$T_m = \frac{T_{\text{min}} + T_{\text{out}}}{2} \tag{3}$$

Using the Churchill–Bernstein rule of external flow across a single tube, the Nusselt number and the exterior convection heat transfer coefficient, h_B, are given as follows:

$$Re = u_f d/\nu_f \tag{4}$$

$$Nu = 0.3 + \frac{0.62Re^{1/2}Pr^{1/3}}{[1 + (0.4/Pr)^{2/3}]^{1/4}}\left[1 + \left(\frac{Re}{282,000}\right)^{5/8}\right]^{4/5} \tag{5}$$

$$h_B = \lambda Nu/d \tag{6}$$

where the wind velocity u_f is 2 m/s and the atmosphere kinematic viscosity ν_f is gained from the diagram of thermophysical property corresponding to the characteristic temperature of atmosphere T_m [16].

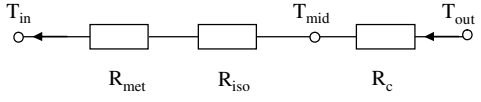

Fig. 2 Sketch of overall thermal resistance.

The exterior convection heat transfer coefficient and heat leakage are calculated iteratively until the following relationship is satisfied:

$$\delta = \frac{|h_A - h_B|}{h_A} \le 0.05 \tag{7}$$

The radiation heat transfer between the tank and atmosphere is expressed as

$$q = C_0[\varepsilon_w(T_w/100)^4 - \varepsilon_g(T_g/100)^4] \tag{8}$$

where the blackbody radiation coefficient C_0 is 5.67 $\text{W}/(\text{m}^2 \cdot \text{K}^4)$.

The total wall heat transfer coefficient is obtained with this calculation of convection and radiation heat transfer, and so the uniform heat flux is treated as a wall condition. In addition, Table 2 gives the parameters of return inlet and feeding pipe outlet under different return inlet locations, which are used as the input parameters for the simulation of the liquid-oxygen tank.

III. Mathematical Model

A. Governing Equations

An energy analysis is used to determine the energy entering into and exiting from the tank in energy conversion systems. The temperature inside the tank varies according to the energy balance. The energy analysis is conducted by solving the continuity, momentum, and energy equations numerically for tank with boundary conditions.

The governing equations in the rectangular coordinate system used for describing flow and heat transfer in the tank and the k–ε turbulence model are given as follows [17]:

Continuity equation:

$$\frac{\partial \rho}{\partial t} + \frac{\partial(\rho u)}{\partial x} + \frac{\partial(\rho v)}{\partial y} = 0 \tag{9}$$

x-momentum equation:

$$\frac{\partial(\rho u)}{\partial t} + u\frac{\partial(\rho u)}{\partial x} + v\frac{\partial(\rho u)}{\partial y} = -\frac{\partial p}{\partial x} + \mu\left[\frac{\partial^2 u}{\partial x^2} + \frac{\partial^2 u}{\partial y^2}\right] \tag{10}$$

y-momentum equation:

$$\frac{\partial(\rho v)}{\partial t} + u\frac{\partial(\rho v)}{\partial x} + v\frac{\partial(\rho v)}{\partial y} = -\frac{\partial p}{\partial y} + \mu\left[\frac{\partial^2 v}{\partial x^2} + \frac{\partial^2 v}{\partial y^2}\right] + \rho g\beta\Delta T \tag{11}$$

Energy equation:

$$\frac{\partial(\rho T)}{\partial t} + \frac{\partial(\rho u T)}{\partial x} + \frac{\partial(\rho v T)}{\partial y} = \frac{\lambda}{c_p}\left[\frac{\partial^2 T}{\partial x^2} + \frac{\partial^2 T}{\partial y^2}\right] \tag{12}$$

Turbulent kinetic energy:

$$\frac{\partial(\rho k)}{\partial t} + \frac{\partial(\rho u k)}{\partial x} + \frac{\partial(\rho v k)}{\partial y} = \frac{\partial}{\partial x}\left[\left(\mu + \frac{\mu_t}{\sigma_k}\right)\frac{\partial k}{\partial x}\right] + \frac{\partial}{\partial y}\left[\left(\mu + \frac{\mu_t}{\sigma_k}\right)\frac{\partial k}{\partial y}\right] + G_k - \rho\varepsilon \tag{13}$$

Table 2 Calculated boundary conditions

Computational parameters	Value			
Return inlet location, hi/L	0.1	0.2	0.3	0.4
Fluid void fraction of return inlet, %	38.9	41.2	44.1	48.2
Fluid velocity of return inlet, $\text{m} \cdot \text{s}^{-1}$	0.651	0.801	1.006	1.311
Fluid temperature of return inlet, K	97.69	97.05	96.45	95.76
Fluid mass flux of feeding pipe outlet, kg/s	9.244	11.18	12.988	15.73

G_k represents the production of turbulent kinetic energy and is given by

$$G_k = \mu_t \left\{ 2\left[\left(\frac{\partial u}{\partial x}\right)^2 + \left(\frac{\partial v}{\partial y}\right)^2 \right] + \left(\frac{\partial u}{\partial y} + \frac{\partial v}{\partial x}\right)^2 \right\} \tag{14}$$

Dissipation rate of turbulent kinetic energy

$$\frac{\partial(\rho\varepsilon)}{\partial t} + \frac{\partial(\rho u\varepsilon)}{\partial x} + \frac{\partial(\rho v\varepsilon)}{\partial y} = \frac{\partial}{\partial x}\left[\left(\mu + \frac{\mu_t}{\sigma_\varepsilon}\right)\frac{\partial \varepsilon}{\partial x}\right] + \frac{\partial}{\partial y}\left[\left(\mu + \frac{\mu_t}{\sigma_\varepsilon}\right)\frac{\partial \varepsilon}{\partial y}\right] + C_{1\varepsilon} G_k \frac{\varepsilon}{k} - C_{2\varepsilon}\rho\frac{\varepsilon^2}{k} \tag{15}$$

The turbulent viscosity is computed as follows:

$$\mu_t = \rho C_\mu (k^2/\varepsilon) \tag{16}$$

where the values of the constants in these equations are given as [17]

$$C_\mu = 0.09, \qquad C_{1\varepsilon} = 1.44, \qquad C_{2\varepsilon} = 1.92$$
$$\sigma_k = 1.0, \qquad \sigma_\varepsilon = 1.3$$

B. Computational Fluid Dynamics Model and Its Simplification

The flow structure and heat transfer in the tank are investigated by means of CFD. The divided block meshes are required because of the large dimensional difference between the tank bulk and partial regions; hence, the appropriate mesh generation strategy is adopted that includes the unstructured mesh in the spherical cap and return flow inlet regions, the structured mesh in the core region, and the denser mesh near the wall. A three-dimensional tank mesh that exceeds 300,000 not only results in slow computational speed but is also difficult to be implemented because the relevant physical process of 5.0 s is only simulated for the continuous computation of 24 h. This mean that 10 years is required for the entire simulation of the precooling operation of 5.5 h from ground filling to rocket launching, which makes the three-dimensional model impractical and model simplification necessary. In this study, the simplified two-dimensional model is adopted to simulate the physical field, and the amount of computational cells that distinctly improve the computational speed is only 25,388. Because the tank curvature is small relative to the large bulk, it is reasonable to regard it as a plate. The three-dimensional values for the velocity of the return inlet and the exterior convection heat transfer of the tank are introduced into the two-dimensional model to simulate the temperature and velocity fields; the legitimacy of temperature and velocity distributions in the tank is assured. The primary difference between the two- and three-dimensional models is only that the mass flux is different, but the effect of the mass flux on the temperature distribution is very faint. The key simplified benchmark is that the liquid height and its falling speed must be uniform with three-dimensional conditions for the consideration of legitimacy. In this paper the primary investigation is focused on the temperature and velocity fields, and so the results of the simplified two-dimensional model are true and dependable.

The volume of fluid model in FLUENT is introduced to perform a free interface condition in the tank and the Courant number is used for 0.85. The standard k–ε turbulence model is applied in numerical calculations and the buoyancy is modeled with the Boussinesq approximation. Underrelaxation parameter coupling is treated using the pressure-implicit with splitting of operators algorithm and the corresponding underrelaxation factor is selected to be 0.3 for pressure, 0.7 for momentum, 1.0 for energy equations, and 1 for body force and density. The solution to the problem is obtained using the implicit method in a segregated solver and the discretization of governing equations is achieved by using the standard method for pressure and second-order upwind method.

The solutions are assumed to converge when the following convergence criterion is satisfied by every dependent variable at every grid point in the computational domain:

$$\left| \frac{\varphi^{\text{new}} - \varphi^{\text{old}}}{\varphi^{\text{new}}} \right| \le \phi \tag{17}$$

Hence, φ in general could be any dependant variable. In this study, $\phi = 1\text{e} - 3$ for continuity and momentum equations and $\phi = 1\text{e} - 6$ for energy equations.

C. User-Defined Program

The cryogenic phase transformation phenomena that include the boiling and condensation transition exist in the tank, but FLUENT software is defective in solving the cryogenic phase transformation. To numerically simulate flowfield in a liquid-oxygen tank and account for phase transformation, the appropriate phase change

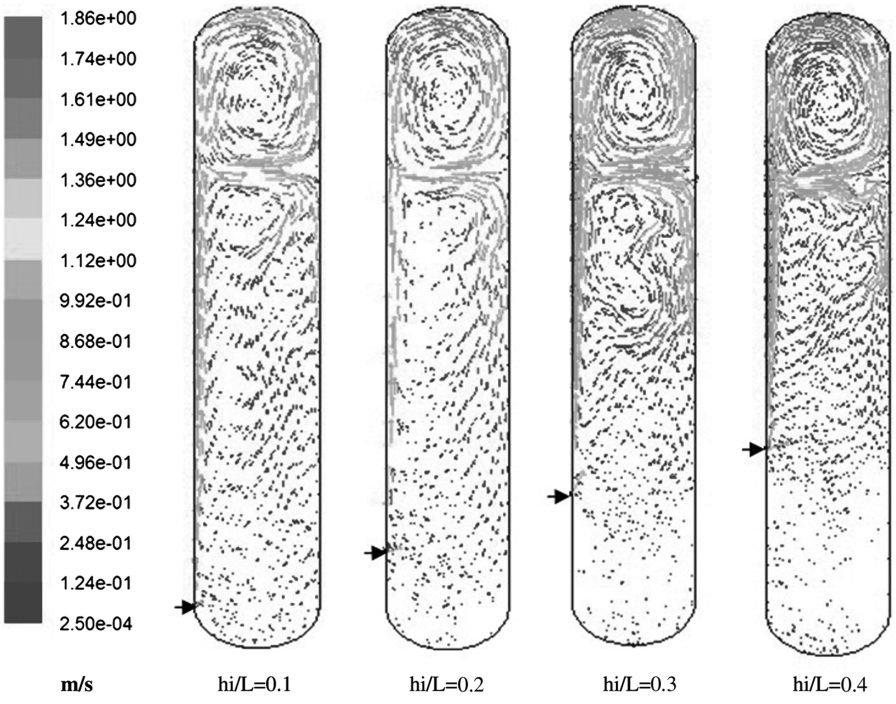

Fig. 3 Sketch of velocity vectors in the tank with different return inlet locations.

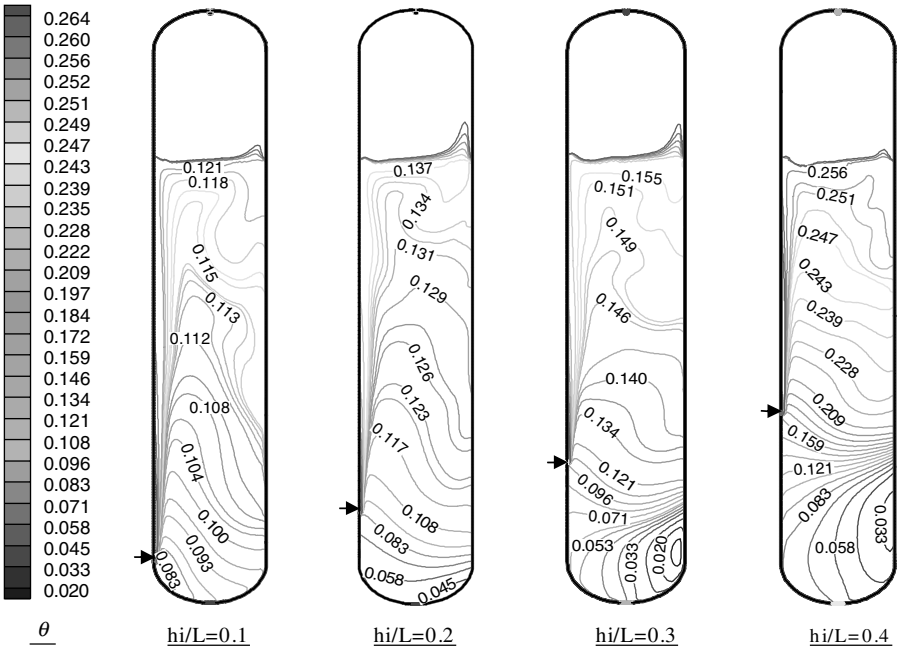

Fig. 4 Isotherms of liquid oxygen in the tank with different return inlet locations.

model must be considered. In this study the user-defined program is compiled to perform the mass and energy transfers.

The mass transfer model is used to solve phase change between the liquid oxygen and vapor oxygen. Evaporation takes place due to the heat absorption from the boiling transition process when the temperature of the liquid oxygen exceeds the saturated value, whereas condensation occurs due to heat releasing for the condensing transition when the temperature of the vapor oxygen is lower than the saturated value. The mass transfer of phase change in the tank includes the evaporation and condensation at the interface, the subcooling boiling of liquid oxygen induced by the wall heat leakage and the return liquid. According to the thermodynamics, the uniform mass transfer of phase change $\dot{m}$ is given by

$$\dot{m} = \frac{\rho V \alpha c_p (T - T_{\text{sat}})}{h_{fg} \Delta \tau} \tag{18}$$

where ρ is the liquid density, V is the cell volume, α is the void fraction, h_{fg} is the latent heat of vaporization, and $\Delta\tau$ is time variable.

IV. Results and Discussion

A. Influence of Return Inlet Location on Thermal Stratification

More complicated operations inside the liquid-oxygen tank during the ground parking are experienced repeatedly, for example, ground self-pressurization, subcooling supply, vapor release, natural circulation precooling, and so on; therefore, the velocity and temperature fields inside the tank go through the intricate changes. The natural circulation precooling operation is dominant during the whole period of ground parking; therefore, this process is focused on the investigation of thermal stratification. Figure 3 describes the velocity vectors in the tank with different return inlet locations after 2 h of natural circulation precooling operation. The return fluid entering into the tank from the precooling loop flows upward under the action of buoyancy force with heated liquid adjacent to the sidewall of the tank. The velocity increases gradually as a result of the same direction of movement and buoyancy force. After reaching the top interface, the gas phase overflows and liquid phase turns toward the opposite wall along the free interface. The fluid again bends downward after approaching the sidewall and it starts losing momentum gently due to viscous and buoyancy effects; hence, the clockwise velocity vortex is presented in the area of the main liquid region. Compared with the velocity vectors in the tank with different return inlet locations, the differences are obvious in the bulk below the return inlet locations where the velocity values descend with the advance of return inlet locations.

It is known from the thermal stratification principle that the heat entering into tank through the sidewall initially assembles in the thermal boundary layer and tends to warm up the liquid oxygen close to the wall. Then the heat in the warm liquid oxygen diffuses with the upward flow of heat fluid, so that the thickness of the thermal boundary layer increases along the tank height and this warm liquid oxygen rises to the surface. Figure 4 gives the isotherms of liquid oxygen in the tank under different return inlet locations after 2 h of natural circulation precooling operation. The top layer of the liquid oxygen is distinctly at a temperature higher than the core of the liquid. When the heat from the ullage space and thermal boundary layer diffuses gradually in the precooling operation, the axial thermal stratification is produced in the main liquid region whereas the radial stratification is distinct below the return inlet location. The convection heat transfer plays an important part in the bulk above the return inlet location because of the intense disturbance, and the heat conduction becomes a more prominent heat transfer mechanism in the bottom region due to the lack of direct effect of return flow; in addition, the velocity value is very low, and so the axial temperature

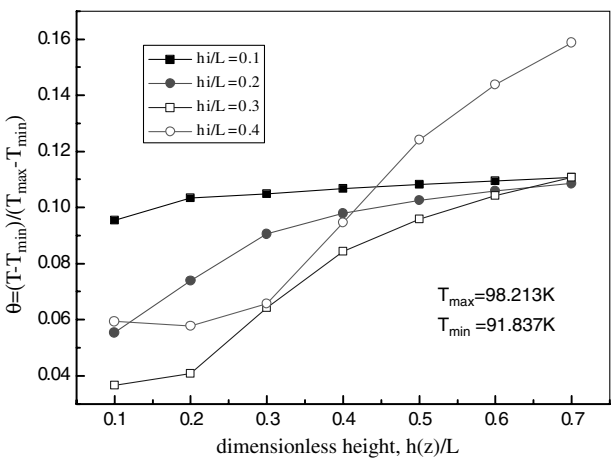

Fig. 5 Variation of region average temperature with different return inlet locations.

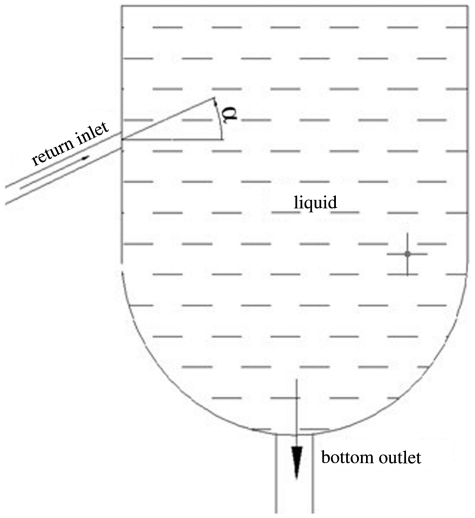

Fig. 6 Schematic diagram of return influx angle.

difference between the bottom and upper region is caused as a result of the modality of heat transfer. It is known from the calculation of the precooling loop that the fluid velocity of the return inlet increases gradually with the elevation of the return locations, and so the disturbance above the return location is enhanced and the convection heat transfer is strengthened. It is clear that the return inlet location at $hi/L = 0.3$ is optimal, at which the volume and the depth of subcooled liquid oxygen in the tank become the largest, correspondingly.

The distribution of the temperature field in the tank is asymmetric because of the return fluid, and so the quantificational investigation of subcooled liquid-oxygen volume is necessary. The average dimensionless excess temperature of different regions along the height with different return inlet locations is shown in Fig. 5. The definition of the dimensionless excess temperature θ and the value selection of $T_{\max}$ and $T_{\min}$ can be seen in the Nomenclature. Obviously the dimensionless excess temperature of liquid oxygen with the return inlet location at $hi/L = 0.3$ is the lowest in the different regions along the height; the subcooling maintained is the most relative to the other cases. From the figure, the effect of the return inlet location on thermal distribution is very distinct and the return inlet location located at $hi/L = 0.3$ above the bottom header is optimal.

B. Influence of Influx Angle on Thermal Stratification

The influence of return inlet location on thermal stratification is very distinct from the above investigation. Moreover, the effect of influx angle on thermal stratification is also sensitive to the field distribution. The tank with the return inlet location at $hi/L = 0.3$ is chosen as the comparative base to study the effect of influx angle on thermal stratification. The influx angle α of the return inlet is defined in Fig. 6 and the angle selected consists of -15, 0, 15, 30, 45, and 60, where the influx angle of -15 deg means declining downward. Figure 7 shows the isotherms of the liquid-oxygen region with different influx angles before the subcooled liquid oxygen supply of ground parking. The distributions of thermal stratification above the return inlet location are similar among the tanks with different influx angles because the return inlet location is settled and so the return inlet velocity is considered to be fixed, whereas distinct differences appear in the regions below the return inlet location. The temperature below the return location with the influx angle of -15 deg is higher comparatively because the return fluid reaches the tank bottom directly and causes the incremental increase in temperature. The axial thermal stratification is dominant in the whole tank with the 30 deg influx angle and the bottom temperature is lower. Comparing with the temperature fields above the return inlet location, the influence of influx angle on the thermal stratification in the bottom is distinct and the influx angle of 30 deg is the perfect selection because of the appearance of maximal subcooling in the tank.

Figure 8 gives the variation of the region average dimensionless excess temperature with different influx angles before the subcooled liquid oxygen supply of ground parking. The liquid-oxygen temperatures in the tank with influx angles of -15 and 15 deg are clearly higher. Although the whole temperature gradient in the tank with the 60 deg influx angle is correspondingly minimal and the upper bulk is at a lower temperature, the quality of liquid oxygen in the tank is low grade because of the decrease in the total subcooling of liquid oxygen

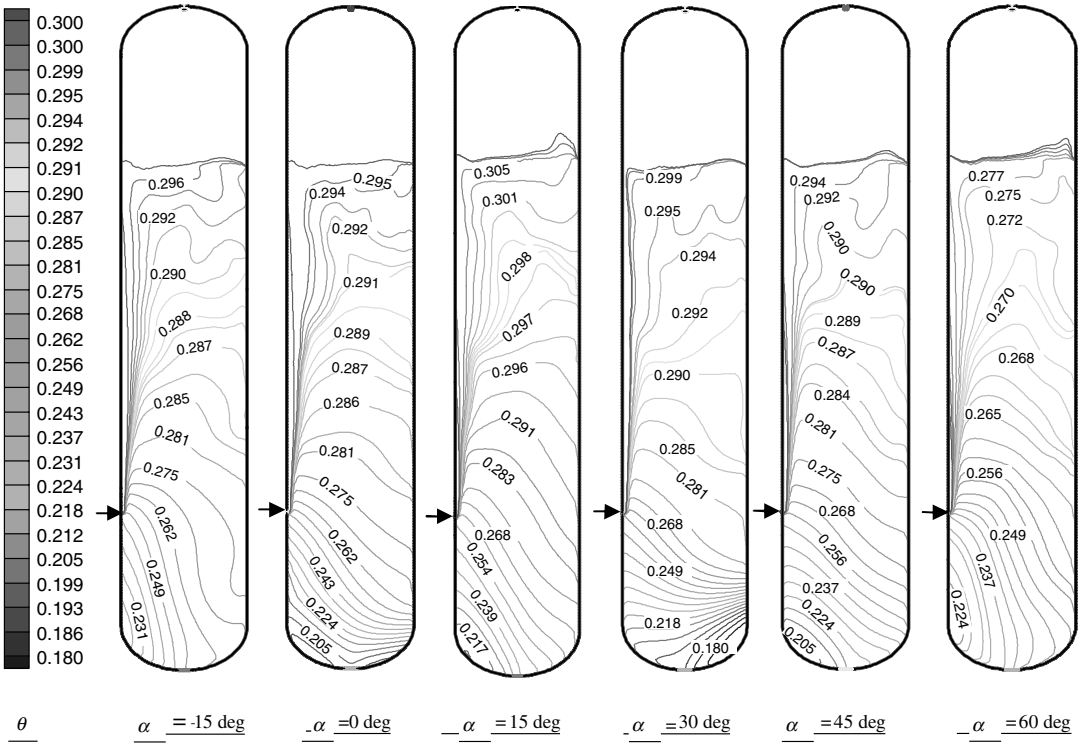

Fig. 7 Isotherms of the liquid-oxygen region in the tank with different influx angles.

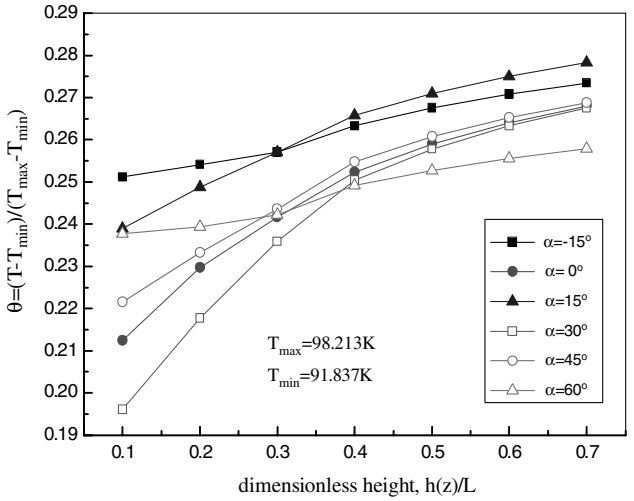

Fig. 8 Variation of region average temperature in the tank with different influx angles.

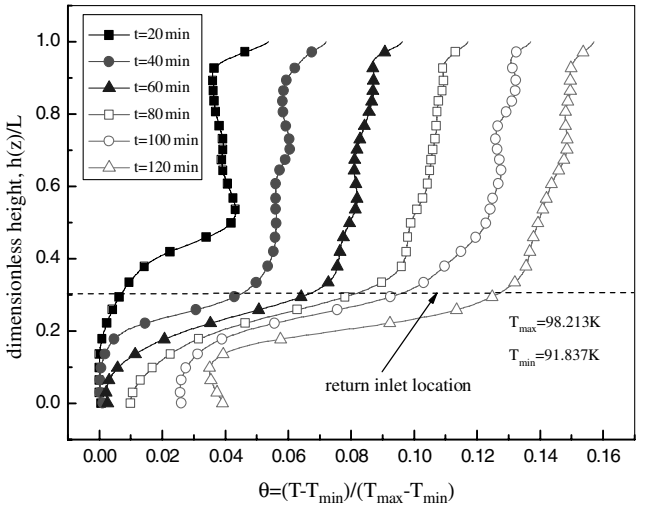

Fig. 10 Variation of centerline temperature with time during natural circulation precooling.

inside the tank. For the comprehensive consideration, the ascending influx angle of 30 deg is the optimal design for which the average temperature and the subcooling of liquid regions have preferable values.

C. Tank with the Optimal Return Inlet Location and Influx Angle

Figure 9 presents the isotherms of the liquid-oxygen region inside the tank with the return location of $hi/L = 0.3$ and an influx angle of 30 deg with time during the natural circulation precooling. After about 20 min of natural circulation precooling, the downward fluid adhering to the right sidewall encounters the return fluid coming from the return loop at the return location; more fluid is pulled toward the upper region and the residual fluid changes to form an anticlockwise velocity vortex in the bottom. Hence, the heat transfers gradually to the return inlet location, the rate of temperature change and temperature gradient improves at the location, and the thermal stratification begins to appear more and more distinctly. The distribution of thermal stratification in the tank bottom begins to change gradually after about 60 min and transforms the axial into the radial after about 100 min. The lowest temperature region appears in the bottom header and moves from one side near the return flow toward the other side with time under the action of anticlockwise velocity vortex; finally, the axial thermal stratification shifts to the radial in the bottom.

The variation of centerline temperature inside the tank with time during the natural circulation precooling process is shown in Fig. 10. The centerline temperature above the return location increases gradually with time and tends to be uniform, but the obvious temperature variation exists in the bottom. The axial temperature gradient below the return inlet location increases gradually with time. This temperature change in the bottom is distinct relative to the upper bulk because of the appearance of an anticlockwise velocity vortex. With the development of anticlockwise velocity vortex, the fluctuation of centerline temperature finally appears along the height direction in the bottom.

The difference in the cross-sectional average dimensionless excess temperature distribution at different heights after 2 h of precooling is shown in Fig. 11. Obviously the temperature profiles above the return inlet location are approximately similar to each other. Moreover, the higher the selected plane, the slower the temperature increment, which is also caused by the different heat transfer mechanisms in the different regions. From Fig. 11, it is known that a uniform whole

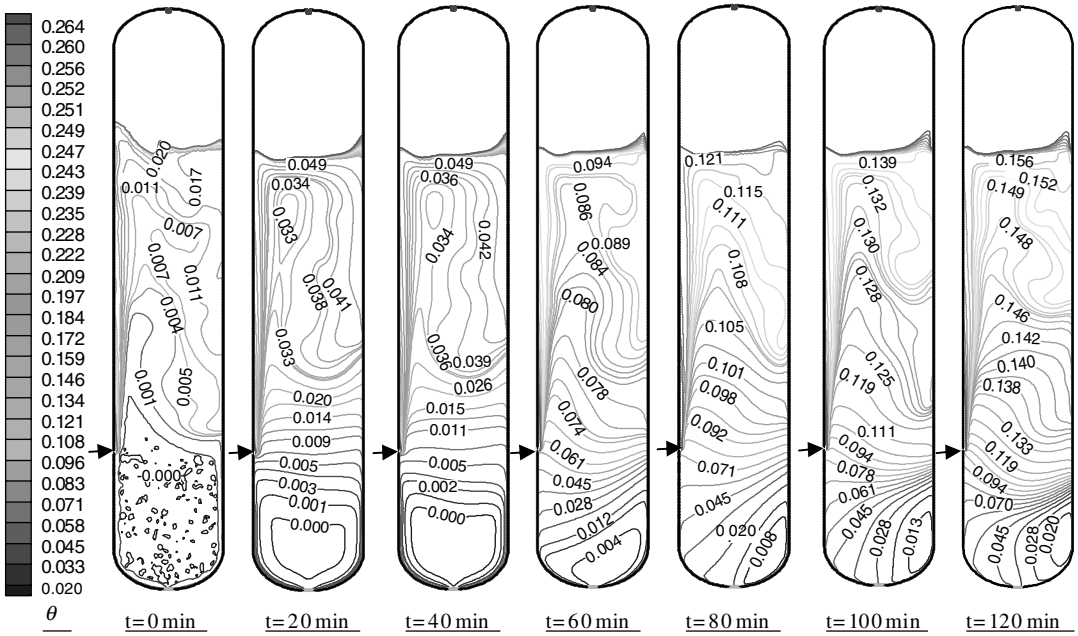

Fig. 9 Isotherms of the liquid-oxygen region with time during natural circulation precooling.

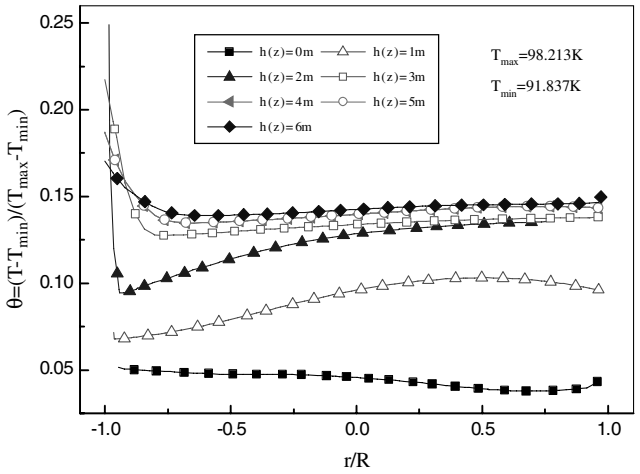

Fig. 11 Cross-sectional average temperature at different heights in the tank after 2 h precooling.

temperature field exists in the region above the return location and the subcooling below the location is larger relative to the upper region. Therefore, the effects of the return inlet location and influx angle on thermal stratification are very distinct.

V. Conclusions

1) The bulk temperature above the return inlet location increases with the rise of the return inlet location and the axial temperature difference enlarges along the height of tank. The optimal value for the return inlet location at $hi/L = 0.3$ and an influx angle of $\alpha = 30$ deg upward are determined, under which the maximal subcooling and the volume of subcooled liquid oxygen are maintained.

2) It is found that the modality of heat transfer in different regions are distinct and the convection heat transfer plays an important part in the bulk above the return flow cross section, whereas heat conduction becomes the dominant heat transfer mechanism in the bottom region due to the shortage of direct effect of return fluid and the velocity value is very small.

3) The anticlockwise velocity vortex is formed in the ullage space while a clockwise vortex is presented in the zone of the liquid phase. The velocity vortex in the bottom region changes from clockwise to anticlockwise, so the lowest temperature region moves from the left side toward the right side of the bottom spherical cap gradually with the heightening of the return flow location.

Appendix: Description of One-Dimensional Homogeneous Unbalance Fluid Dynamic Model

I. Heat Transfer Models Between Pipeline Wall and Cryogenic Liquid

Precooling a pipeline with cryogenic liquid is a typical high-velocity reflooding heat transfer process. Figure A1 presents the typical flow regimes and the corresponding heat transfer regions of the high-velocity reflooding process in a vertical pipeline [18]. As shown in Fig. A1, the flow regimes may undergo the transition from fully liquid flow, bubble flow, slug flow, inverted annular flow, dispersed flow to fully gas flow, and the corresponding heat transfer regions are fully liquid convective heat transfer, subcooled boiling, saturated nucleate boiling, inverted annular film boiling, dispersed film boiling and fully gas flow. The transition from inverted annular flow to dispersed flow is an especially important flow phenomenon. At the beginning of the heated section, where the vapor fraction occupies a small proportion, the flow is annular with the liquid in the center and the vapor in the annulus. Because of the large velocity increase caused by the generation of low-density vapor, the drag force on the liquid core increases at greater tube lengths to the point that the core is torn apart into filaments and droplets of liquid. As the breakup continues, the flow goes through a somewhat gradual

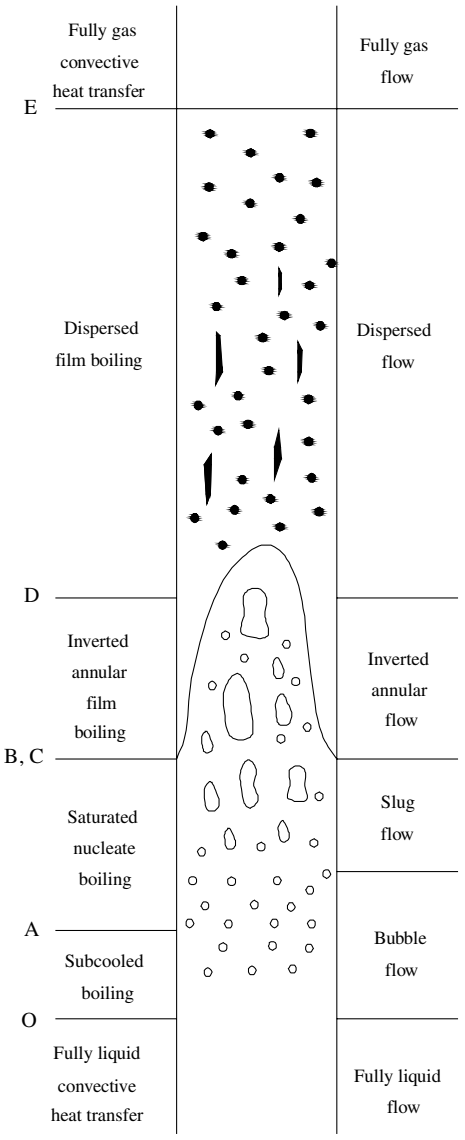

Fig. A1 Flow regimes and heat transfer regions of high-velocity reflooding process in vertical pipelines.

transition to a dispersed flow regime in which small droplets and filaments of liquid are carried along in a vapor matrix.

Figure A2 shows the boiling curve of the high-velocity reflooding process, which belongs to a temperature-controlled boiling process [18]. It includes seven heat transfer stages: fully liquid convective heat transfer, subcooled boiling, saturated nucleate boiling, inverted annular transition boiling, inverted annular film boiling, dispersed film boiling and fully gas convective heat transfer. Point B is the first critical point and the maximum heat flux point of nucleate boiling. Point C is the second critical point and the minimum heat flux point to maintain film boiling. Compared with Fig. A1, an instantaneous inverted annular transition boiling stage (C–B) is added to depict the transition from the inverted annular film boiling to the saturated nucleate boiling, which means that the vapor film vanishes and cryogenic liquid first contacts with the pipeline wall as the vapor film cannot sustain the weight of liquid layer. It is an unstable and transient heat transfer process and usually ignored by previous researchers, which makes the physical meaning of precooling process discontinuous. A linear interpolation method between the maximum heat flux of nucleate boiling and the minimum heat flux of film boiling is adopted to simulate the inverted annular transition boiling process. Considering the high heat flux at point B, the predicted transition time is very short and accords with the actual transition process. Based on the aforementioned flow and heat transfer analysis of the high-velocity reflooding process, one set of

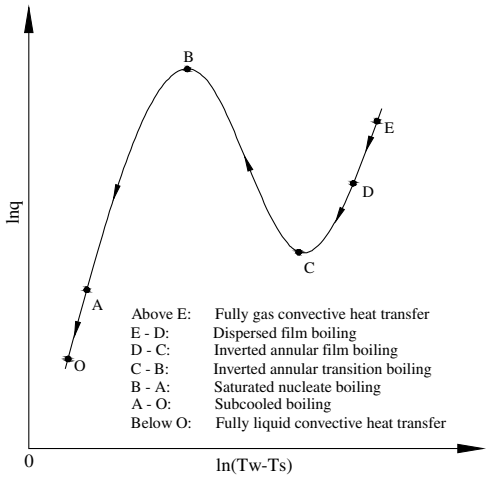

Fig. A2 Boiling curve of high-velocity reflooding process.

heat transfer models between the pipeline wall and cryogenic liquid was established [19].

II. One-Dimensional Unsteady Homogeneous Models of Natural Circulation Precooling

The unsteady flow and heat transfer characteristics of the natural circulation precooling loop of cryogenic liquid rocket engine were analyzed with a one-dimensional homogeneous model. To simplify the computations, some assumptions were developed as follows:

1) The flow in the natural circulation loop is a one-dimensional channel flow, and the loop is in quasi-steady state at any precooling time. The pressure fluctuation in the precooling process is not considered and deems that the pressures at the inlet position and at the backward position of the loop are the local static pressure.

2) Only one-dimensional radial heat transfer of metal walls and insulation layers are considered, whereas the axial heat transfer of the pipelines is ignored.

3) The liquid and gas phases are well mixed and in heat balance.

For one-dimensional channel flow, the time-dependent mass, momentum, and energy conservation equations and the equation of state can be expressed as follows:

Continuity:

$$\frac{\partial \rho}{\partial t} + \frac{\partial(\rho u)}{\partial z} = 0 \tag{A1}$$

Momentum conservation:

$$\frac{\partial(\rho u)}{\partial t} + \frac{\partial(\rho u^2)}{\partial z} = -\frac{\partial p}{\partial z} - \frac{\partial p_f}{\partial z} - \rho g \cos\theta \tag{A2}$$

Energy conservation:

$$\frac{\partial(\rho h)}{\partial t} + \frac{\partial(\rho u h)}{\partial z} = -p\frac{\partial u}{\partial z} + \frac{P_i}{A} h_w (T_w - T_f) \tag{A3}$$

State:

$$\rho_l = \rho_l(p, T), \qquad \rho_g = \rho_g(p, T) \tag{A4}$$

where ρ, p, T, u, and h indicate the average density, pressure, temperature, uniform velocity, and average enthalpy of the cryogenic fluid, respectively. In addition, g is the acceleration due to gravity, θ is the angle of the flow direction from the horizontal plane, T_w is the inner wall temperature, h_w is the heat transfer coefficient between the pipeline wall and cryogenic liquid, and P_i and A represent the inside perimeter and cross-sectional area of the pipeline, respectively. Frictional pressure loss p_f in the momentum conservation equation is computed by the Lockhart–Martinelli correlation formula.

Considering the obvious radial temperature gradient between the metal wall and insulation layer, the one-dimensional transient radial heat release equation of the circulation loop is formulated by

$$\frac{\partial T_r}{\partial t} = \frac{\lambda_w}{\rho_w c_{pw}} \left(\frac{\partial^2 T_r}{\partial r^2} + \frac{1}{r}\frac{\partial T_r}{\partial r} \right) - \frac{P_i}{\rho_w c_{pw} A} h_w (T_w - T_f) \tag{A5}$$

where T_r, r, λ_w, ρ_w, and c_{pw} are the grid temperature along the radial direction, radial coordinate, heat conduction coefficient, density, and specific heat capacity at constant pressure of the pipeline material, respectively. The radial heat release equation of the circulation loop and the flow and heat transfer equations of the cryogenic liquid are coupled by the heat transfer coefficient h_w between the pipeline wall and cryogenic liquid.

The solution of the unsteady circulation flow rate is a focus in the unsteady natural circulation precooling process. Based on the earlier assumption in Eq. (1), the pressures at the bottom outlet and the return inlet of the loop are the local static pressure; furthermore, it makes the calculation of unsteady circulation flow rate feasible by bisection method. At every moment t, the iterative interval $[v_0 - \Delta v, v_0 + \Delta v]$ of the inlet velocity of the feed pipeline is first determined according to the inlet velocity v_0 at the previous moment $(t - \Delta t)$. Next, by judging the heat transfer region of each cell along the flow direction, the heat flux from the pipeline to the cryogenic liquid, frictional pressure loss, gravity pressure loss, acceleration pressure loss, pressure, temperature, and mass fraction of gas phase in every flow cell are computed. When the calculated pressure at the return inlet location is close to approaching the actual local static pressure in the LO_2 tank ($\Delta p < 10^{-6}$ bar), the inlet velocity v_0 will be considered as the actual inlet velocity of the feed pipeline at moment t; otherwise, the iterative process will be continued.

III. Grid Arrangement of Natural Circulation Loop

An equally spaced grid arrangement is adopted along the flow direction. The changing time step of the initial precooling process is determined by the grid step and the mass flux of the circulation loop, and until the flow arrives at the return inlet location, the time step will be a fixed value of 0.1 s. Because of the high radial temperature gradient between the metal wall and insulation layer, the radial direction of the pipeline is divided into many cells as well. In the pump pipeline, for example, the schematic diagram of grid arrangement is shown in Fig. A3. According to the computation requirements, the gird step along the flow direction is 0.002 m, the axial node number is 9666, and the radial node number is 23.

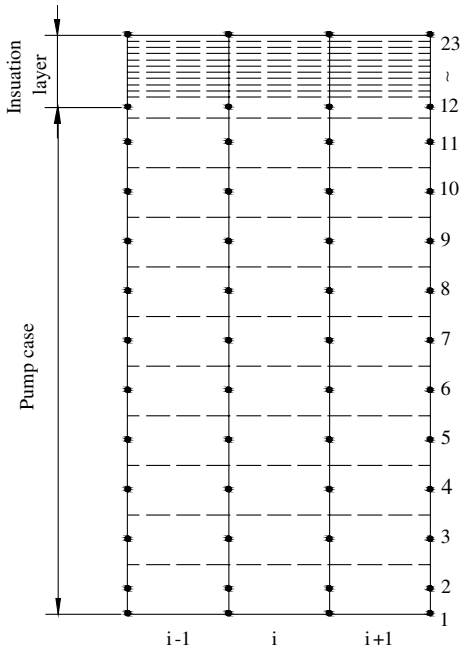

Fig. A3 Schematic diagram of grid arrangement of pump pipeline.

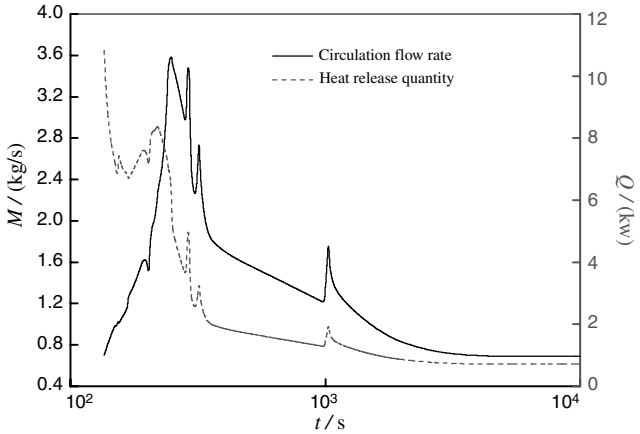

Fig. A4 Circulation mass flux and heat release quantity during the precooling with a return location of $hi/L = 0.1$.

IV. Flow Characteristics of Natural Circulation Precooling Loop

The driving force of the natural circulation loop can be directly expressed by the circulation flow rate during precooling. Figure A4 shows the predicted circulation flow rate and the heat release quantity of the circulation loop in the precooling process. Overall, the predicted circulation flow rate increases at first and then decreases to the steady value, and there are several peak values of circulation flow rate during precooling. These can be interpreted by the heat release quantity transferred to the cryogenic liquid from the circulation loop.

The precooling phenomenon of a pipeline is a temperature-controlled boiling process. Figure A5 shows the boiling curves of the two-phase oxygen at a different mass fraction of the gas phase. Herein, the horizontal axis indicates the wall superheat, whereas the vertical axis indicates the heat flux between the pipeline node and the cryogenic liquid. With the decreasing of wall superheat, each node of the circulation loop will undergo the transition process from film boiling, transition boiling, and nucleate boiling to the single-phase convective flow. In Fig. A5, point B is the first critical point and the maximum heat flux point of nucleate boiling. Point C is the second critical point and the minimum heat flux point to maintain film boiling. According to the boiling curves, the heat flux between the pipeline node and cryogenic liquid will decrease first before point C, and then increase between points C and B, eventually continuing to decrease to the lower single-phase convective heat flux after point B. Considering the instantaneous transition boiling, the heat release quantity transferred to the cryogenic liquid from the circulation loop is decreasing at most times. Only when the transition from film to nucleate boiling occurs at a particular pipeline, can the peak value of the heat release quantity be developed. As shown in Fig. A4, three peak values of the heat release quantity during precooling are presented after 250 s, which indicates the transition of heat transfer mechanisms at the pipeline between the engine entrance and main pump entrance, the pipeline between the pump exit and blowdown valve, and the pump pipeline, respectively. The unsteady characteristics of the heat release quantity during the precooling eventually bring on the peak features of the circulation flow rate. On the other hand, because the heat release quantity of the loop circulation is high and gas oxygen appears in the supply pipeline at the initial precooling stage, the liquid density contrast between the feed pipeline and the return pipeline will be small and the circulation flow rate will increase as the heat release quantity of the loop decreases. In succession, when the vapor oxygen disappears in the feed pipeline, the circulation flow rate will diminish with a decrease in the heat release quantity of the circulation loop. Eventually, the natural circulation precooling process will become stable after about 40 min. Above all, the circulation flow rate in the precooling process, that is, the driving force of the natural circulation loop, will show a trend of first increasing and then decreasing, and there are several peak values of circulation flow rate when the transition from film to nucleate boiling occurs at particular pipelines.

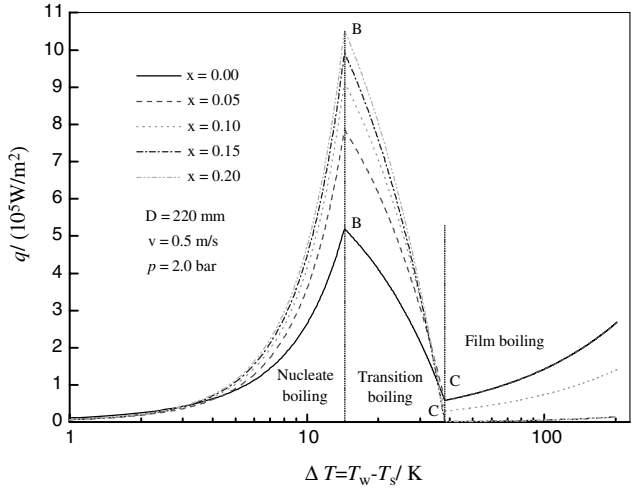

Fig. A5 Boiling curves at different mass fractions of the gas phase.

Acknowledgments

The paper is supported by the Specialized Research Fund for the Doctoral Program of Higher Education by the Ministry of Education (20060698021). The author would like to thank the Ministry of Education, People's Republic of China, for their financial support.

References

[1] Clark, J. A., "A Review of Pressurization, Stratification, and Interfacial Phenomena," *Advances in Cryogenic Engineering*, Vol. 10, Plenum, New York, 1965, pp. 259–283.

[2] Bailey, T. E., and Fearn, R. F., "Analytical and Experimental Determination of Liquid-Hydrogen Temperature Stratification," *Advances in Cryogenic Engineering*, Vol. 9, 1964, pp. 254–264.

[3] Lin, C. S., and Hasan, M. M., "Numerical Investigation of the Thermal Stratification in Cryogenic Tanks Subjected to Wall Heat Flux," AIAA Paper 1990-2375, 1990.

[4] Khurana, T. K., Prasad, B. V. S. S. S., Ramamurthi, K., and Murthy, S. S., "Thermal Stratification in Ribbed Liquid Hydrogen Storage Tanks," *International Journal of Hydrogen Energy*, Vol. 31, 2006, pp. 2299–2309. doi:10.1016/j.ijhydene.2006.02.032

[5] Navickas, J., and Douglas, M., "Prediction of a Liquid Tank Thermal Stratification by a Finite Difference Computing Method," AIAA Paper 1988-2917, 1988.

[6] Zhang, T. Y., and Li, S. M., "Numerical Simulation for Thermal Stratification of Liquid Hydrogen," *Journal of Zhejiang University*, Vol. 26, No. 1, 1992, pp. 98–103.

[7] Das, S. P., Chakraborty, S., and Dutta, P., "Studies on Thermal Stratification Phenomenon in LH2 Storage Vessel," *Heat Transfer Engineering*, Vol. 25, No. 4, 2004, pp. 54–66. doi:10.1080/01457630490443767

[8] Tatom, J. W., Brown, W. H., Knight, L. H., and Coxe, E. F., "Analysis of Thermal Stratification of Liquid Hydrogen in Rocket Propellant Tanks," *Advances in Cryogenic Engineering*, Vol. 9, 1964, pp. 265–272.

[9] Manalo, L., "A Numerical Study of Thermal Stratification Due to Transient Natural Convection in Densified Liquid Propellant Tanks," Ph.D. Thesis, Univ. of New Orleans, New Orleans, LA, 2003.

[10] Altuntop, N., Kilik, Z., Ozceyhan, V., and Kincay, O., "Effect of Water Inlet Velocity on Thermal Stratification in a Mantled Hot Water Storage Tank," *International Journal of Energy Research*, Vol. 30, 2006, pp. 163–176. doi:10.1002/er.1134

[11] Knudsen, S., and Furbo, S., "Thermal Stratification in Vertical Mantle Heat Exchangers with Application to Solar Domestic Hot-Water Systems," *Applied Energy*, Vol. 78, 2004, pp. 257–272. doi:10.1016/j.apenergy.2003.09.002

[12] Kenjo, L., Inard, C., and Caccavelli, D., "Experimental and Numerical Study of Thermal Stratification in a Mantle Tank of a Solar Domestic Hot Water System," *Applied Thermal Engineering*, Vol. 27, 2007, pp. 1986–1995. doi:10.1016/j.applthermaleng.2006.12.008

[13] Altuntop, N., Arslan, M., Ozceyhan, V., and Kanoglu, M., "Effect of Obstacles on Thermal Stratification in Hot Water Storage Tanks,"

Applied Thermal Engineering, Vol. 25, 2005, pp. 2285–2298. doi:10.1016/j.applthermaleng.2004.12.013

[14] Shin, M. S., Kim, H. S., Jang, D. S., Lee, S-M., Lee, Y-S., and Yoon, H-G."Numerical and Experimental Study on the Design of a Stratified Thermal Storage System," *Applied Thermal Engineering*, Vol. 24, 2004, pp. 17–27. doi:10.1016/S1359-4311(03)00242-4

[15] Chen, E. F., Li, Y. Z., Cheng, X. H., and Yu, F., "Unsteady Mathematic Models of Natural Circulation Loop Precooling of Liquid Rocket Engine," *Journal of Xi'an Jiaotong University*, Vol. 42, No. 9, 2008, pp. 1127–1131.

[16] Yang, S. M., and Tao, W. Q., *Heat Transfer*, 4th ed., Higher Education Press, Beijing, 2006.

[17] Tao, W. Q., *Numerical Heat Transfer*, 2nd ed., Xi'an Jiaotong Univ. Press, Xi'an, People's Republic of China, 2002.

[18] Lu, Z. Q., *Two Phase Flow and Boiling Heat Transfer*, Tsinghua Univ. Press, Beijing, 2002.

[19] Chen, E. F., Li, Y. Z., Cheng, X. H., and Li, C., "Numerical Research on High Velocity Reflooding Heat Transfer Process of Cooling Down," *Journal of Huazhong University of Science and Technology*, Vol. 37, No. 2, 2009, pp. 104–107.